Journal of Power Sources 543 (2022) 231839

Contents lists available at ScienceDirect

Journal of Power Sources

journal homepage: www.elsevier.com/locate/jpowsour

Long-term stable Li metal anode enabled by strengthened and protected lithiophilic LiZn alloys

Yongfang Lai, Hongyu Zhang, Guanglin Xia *, Xuebin Yu **

Department of Materials Science, Fudan University, Shanghai, 200433, China

HIGHLIGHTS

- Strengthened and protected LiZn alloys is realized by building $[LiNBH]_n$ chains.
- Polymer-like $[LiNBH]_n$ chains facilitate Li plating into LiZn alloys.
- Polymer-like $[LiNBH]_n$ chains alleviate the volume change of LiZn alloys.
- The thus-fabricated anode delivers an ultralong lifespan of 1200 h at 5 mA cm^{-2}.

ARTICLE INFO

Keywords:
Li metal anode
Li-ion batteries
Li dendrites
Hybrid protective layer
Full cells

ABSTRACT

Li metal are regarded as one of the most promising anodes for next-generation rechargeable batteries. The continuous growth of Li dendrites, however, remains a big challenge for the practical application of Li metal anodes. Herein, an artificial solid-electrolyte interphase layer composed of lithiophilic LiZn alloys under the protection and strengthening of polymer-like $[LiNBH]_n$ chains with high Li ion conductivity is built to develop long-term dendrite-free Li metal anodes. The lithiophilic LiZn alloys, acting as homogeneous nucleation sites, effectively reduce the nucleation barrier for Li plating and hence promote uniform Li plating and stripping process. Simultaneously, the homogeneous layer of polymer-like $[LiNBH]_n$ chains with high Li ion conductivity that are uniformly built inside of LiZn alloys and on the surface of LiZn alloys facilitates Li diffusion down into LiZn alloys and simultaneously alleviate the volume change of LiZn alloys during long-term Li plating and stripping process. Impressively, the thus-fabricated anode delivers an ultralong lifespan of 1200 h at 5 mA cm^{-2} with a fixed capacity of 5 mA h cm^{-2}. By pairing with commercial $LiFePO_4$ cathode, the thus-assembled full cell exhibits a specific capacity of 133 mA h g^{-1}, corresponding to a capacity retention of 88%, at 1 C after 400 cycles.

1. Introduction

Metallic Li, which exhibits an ultrahigh theoretical specific capacity of 3860 mA h g^{-1} and the ultralow electrochemical potential (−3.040 V *vs* standard hydrogen electrode), has been widely regarded as an ideal anode material for next-generation energy storage systems with high energy density [1–4]. The practical application of Li metal anodes, however, is significantly hindered by the uncontrollable growth of Li dendrites [5–7]. The continuous accumulation of isolated Li dendrites during repeated Li plating process could generate numerous “dead Li” layer on the surface of Li metal anode, resulting in the increase of voltage polarization and the continuous capacity degradation [8–11]. More importantly, the electrolyte could spontaneously react with Li that has high chemical reactivity, leading to the formation of solid electrolyte interphase (SEI), which is originally brittle and fragile that could be usually cracked by the large volume change during repeated Li stripping and plating process [12–14]. The thus-exposed fresh Li underneath would constantly consume electrolyte, and the repeated fracture and repair of SEI could finally result in the depletion of electrolyte and Li, which accelerates the failure of batteries. Furthermore, the locally enhanced ion flux at the cracks could further induce nonuniform Li deposition and hence trigger the fast growth of Li dendrites.

* Corresponding author.
** Corresponding author.
E-mail addresses: xiaguanglin@fudan.edu.cn (G. Xia), yuxuebin@fudan.edu.cn (X. Yu).

https://doi.org/10.1016/j.jpowsour.2022.231839
Received 11 April 2022; Received in revised form 2 July 2022; Accepted 6 July 2022
Available online 11 July 2022

In order to tackle these issues caused by Li dendrites and infinite side reaction between Li and electrolyte, considerable efforts have been made, including the introduction of three-dimensional (3D) hosts [15–17], the building of artificial SEI [18–23], and the optimization of electrolytes [24–27]. The introduction of inactive frameworks as 3D hosts, however, would reduce the theoretical specific capacity of thus-built Li metal anodes, leading to the tremendous decrease of energy density. In addition, the large surface area of 3D hosts could increase the contact area between Li metal and electrolyte, which could exacerbate side reactions between them and hence promote the depletion of electrolyte and Li metal and the eventual failure of batteries. In addition, the decomposition of isosorbide dinitrate as the additive of the electrolytes could enrich the SEI with abundant LiN_xO_y and hence induce uniform Li deposition [28]. Although the optimization of electrolytes *via* introducing additives could suppress the growth of Li dendrites to some extent, this strategy is not suitable for achieving long-term cycling stability of Li metal anodes due to the continuous consumption of these additives during Li stripping and plating process. Comparatively, it has been demonstrated that the building of artificial SEI layers with Li-rich alloys, which is capable of effectively reducing the nucleation barrier for Li plating, could suppress the vertical growth of dendritic Li [29–32]. Although these artificial SEI layers play an important role in regulating the Li plating behavior, the intrinsic and large volume change of Li-rich alloys during cycling Li stripping and plating process is still capable of breaking these fragile SEI layers, especially at high current densities and areal capacities. Taking advantage of rigid hypercrosslinked skeletons with excellent flexibility and uniform Li ion diffusion ability, novel all-organic protective layers based on polymer brushes have also been proposed as artificial SEI films, which enables Li metal anodes to deliver stable Li plating and stripping performance for more than 2800 h under a high areal capacity of 10 mA h cm^{-2} [33,34]. More recently, an artificial SEI layer of polymer-like $[LiNBH]_n$ chains with high Li ion conductivity is developed to induce the uniform Li plating process and protect Li metal from the corrosion of the electrolyte [35]. Only limited cycling stability, however, could be obtained owing to the large volume change involved during Li plating and stripping process and the limited lithiophilicity of $[LiNBH]_n$ chains. Therefore, building a robust artificial SEI layer with high lithiophilicity and Li ion conductivity is of great significance but a great challenge for inhibiting the growth of Li dendrites and enabling long-term cycling stability of Li metal anodes.

In this work, an artificial SEI layer, composed of lithiophilic LiZn alloys serving as the lithiophilic sites [36–38], which is subsequently strengthened and protected by polymer-like $[LiNBH]_n$ chains with high Li ion conductivity, is built to develop dendrite-free Li metal anodes with long-term cycling stability. Lithiophilic LiZn alloys is first fabricated on the surface of Li metal *via in-situ* reaction between Li and diethylzinc, with the formation of LiH as the by-product that are uniformed distributed inside of thus-formed LiZn alloys [39]. This unique structure enables the strengthening and protection of lithiophilic LiZn alloys *via* the uniform formation of polymer-like $[LiNBH]_n$ chains with high Li ion conductivity that is achieved by *in-situ* reaction between LiH and ammonia borane followed by thermal heating. Therefore, not only the volume change and the corrosion of lithiophilic LiZn alloys, which could significantly lower the nucleation barrier of Li plating, could be effectively alleviated, but also the homogeneous Li ions diffusion could be realized due to the high Li ion conductivity of polymer-like $[LiNBH]_n$ chains as the protective layer, which promotes Li plating down into lithiophilic LiZn allys. As a result, the thus-modified Li metal anodes by strengthened and protected lithiophilic LiZn alloys (denoted as LiNBH@Zn@Li) exhibit stable voltage polarization (~9 mV) at a current density of 1 mA cm^{-2} for 3200 h. Impressively, upon increasing the current density to 5 mA cm^{-2} with a deep stripping and plating capacity of 5 mA h cm^{-2}, an ultralong lifespan of 1200 h could still be achieved for LiNBH@Zn@Li anode. Furthermore, upon coupling LiNBH@Zn@Li anode with commercial $LiFePO_4$ (LFP; 10.5 mg cm^{-2}) cathode, the thus-assembled full cell delivers a high specific capacity of 133 mA h g^{-1}, corresponding to a capacity retention of 88%, at 1 C after 400 cycles.

2. Experimental section/methods

Preparation of Zn@Li anode: Commercial Li foil anode was first scraped to remove the oxide layer on its surface to facilitate subsequent reactions. The fabrication of LiZn alloy layer on the Li foil (denoted as Zn@Li) was realized by dipping Li foil (9 mm in diameter) into a solution of diethylzinc and then heated at the temperature of 150 °C for several seconds.

Preparation of LiNBH@Zn@Li anode: A amount of 0.05 M AB/THF (ammonia borane dissolved in tetrahydrofuran) was dripped by pipette onto the surface of the thus-obtained Zn@Li electrode, which was further heated at 80 °C for 5 min, followed by natural cooling down to the ambient temperature. Subsequently, this electrode was heated up to 150 °C for hydrogen desorption to obtain the LiNBH@Zn@Li anode.

Materials characterization: The phase structure of LiNBH@Zn@Li and Zn@Li anode was measured by X-ray diffraction (XRD, D8 Advance, Bruker AXS Corporation) with Cu Kα radiation ($\lambda = 1.5418$ Å). Top-view and side-view images of LiNBH@Zn@Li, Zn@Li and bare Li anode were obtained by a field-emission scanning electron microscope (FE-SEM; JEOL 7500FA, Tokyo, Japan). X-ray photoemission spectroscopy (XPS) experiments were performed on Thermo Scientific K-Alpha$^+$ with single X-ray source, using an Al Kα (1486 eV) anode. All binding energies were calibrated by using the contaminant carbon (C 1s = 284.8 eV) as a reference. The surface chemical environment of the modified anode was further investigated by the fourier-transform infrared (FT-IR; Magna-IR 550, Nicolet) spectra. A small spoon was used to carefully scrape off the modified layer on the surface of LiNBH@Zn@Li anode, and then the scraped powder was mixed completely for X-ray diffraction as well as the fourier-transform infrared spectra.

Electrochemical measurement: CR2032 type coin cells and Celgard 2400 pp membrane separator were used to assemble all the tested cells. All the cells were assembled in an argon-filled glovebox. In symmetric cells, 1 M LiTFSI in 1,3-dioxolane (DOL) and dimethoxyethane (DME) (1:1 in volume) with 0.2 M $LiNO_3$ was employed as the ether-based electrolyte. Carbonate-based electrolyte used in this work was 1 M $LiPF_6$ in ethyl carbonate (EC) and diethyl carbonate (DEC) (1:1 in volume) with the addition of 10 wt% fluoroethylene (FEC) and 1 wt% vinylene carbonate (VC). 1 M $LiPF_6$ in ethyl carbonate (EC) and diethyl carbonate (DEC) (1:1 in volume) with the addition of 10 wt% fluoroethylene (FEC) was used in full cells coupling with LFP (LFP:10.5 mg cm^{-2}). In each tested cells, the volume of electrolyte was controlled around 30 μL. The mass loading of LFP cathode was about 10.5 mg cm^{-2} and the mass loading of S cathode was about 1.5 mg cm^{-2}. All the tested electrodes, including LiNBH@Zn@Li, Zn@Li and bare Li, were punched into disks with a diameter of 9 mm in symmetric cells and 12 mm in full cells, respectively.

Electrochemical performance was investigated in a galvanostatic mode at various current densities using a LAND battery tester. The electrochemical impedance spectroscopy (EIS) and the corresponding exchange current density measurements were performed on a Biologic VMP-3 electrochemical workstation. The voltage window was 2.5–4 V for full cells using LFP as the cathode and 1.7–2.8 V for full cells using S as the cathode. EIS tests were conducted in the frequency range from 100 kHz to 0.1 kHz and linear sweep voltammetry (LSV) was performed in a range between −200 and 200 mV versus Li^+/Li at a fixed sweep rate of 1 mV s^{-1}.

3. Results and discussion

As schematically illustrated in Fig. 1a, a uniform layer of lithiophilic LiZn alloys is first built on the surface of Li foil (denoted as Zn@Li) based on the *in-situ* reaction between Li and diethylzinc upon heating at 150 °C for several seconds, with the formation of LiH as the by-product that are

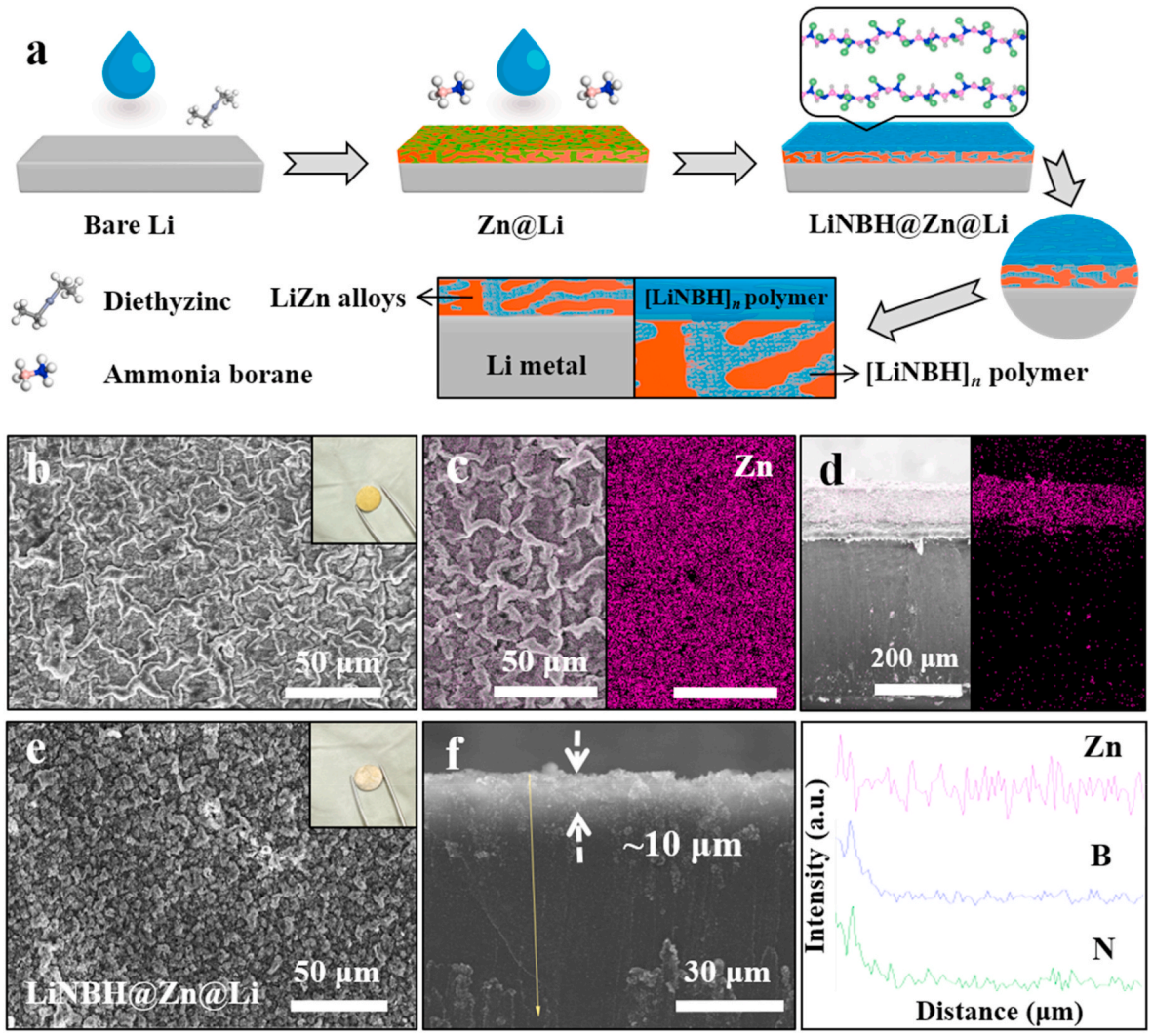

Fig. 1. (a) Schematic illustration for the fabrication of the LiNBH@Zn@Li anode. (b) Top-view SEM image (inset: the optical photograph of the as-fabricated Li meal anode). (c) Elemental mapping results and (d) cross-sectional SEM image of the as-prepared Zn@Li anode. (e) Top-view SEM image and (f) cross-sectional and the corresponding line scanning element analysis of the as-prepared LiNBH@Zn@Li anode.

uniformly dispersed inside of LiZn alloys. After this procedure, the fourier-transform infrared (FTIR) spectra (Fig. 2a) validate the existence of LiH and X-ray diffraction (XRD) pattern (Fig. 2b) demonstrates the formation of LiZn alloys, which provides direct evidence to the formation of LiZn alloys and LiH resulting from the chemical reaction between Li and diethylzinc. Additionally, the chemical environment of the surface of Zn@Li was investigated in detail by high-resolution Li 1s X-ray photo-electron spectroscopy (XPS). The characteristic peaks of 53.9 eV and 55.5 eV the Li 1s spectrum could be attributed to Li–Zn of LiZn alloys and Li–H bond of LiH (Fig. S1), which agrees well with the observation of LiZn alloys and LiH as the by-products. Scanning electron microscopy (SEM) images and the related elemental mapping results illustrate the uniform formation of LiZn alloys and LiH on the surface of Zn@Li (Fig. 1b–d and Fig. S2) with a thickness of ~10 μm as evidenced by cross-sectional SEM image (Fig. S3).

Subsequently, the as-formed LiZn alloys is strengthened and protected by the uniform synthesis of a polymer-like $[LiNBH]_n$ chains, which is realized through *in-situ* reaction between LiH and ammonia borane (AB) solution, followed by thermal heating for H_2 desorption-induced polymerization. Owing to the uniform distribution of LiH inside of the thus-formed LiZn alloys and the favorable interaction between LiH and AB (*i.e.*, $LiH + NH_3BH_3 \rightarrow LiNH_2BH_3 + H_2$) [40–42], the uniform formation of $LiNH_2BH_3$, as verified by the detection of characteristic peaks of B–H bonds and N–H bonds and the disappearance of LiH (Fig. 2a), is expected on the surface of Zn@Li (denoted as LiAB@Zn@Li). After facile H_2 desorption, FTIR spectra validates the significant decrease of B–H and N–H peaks, accompanied by the increase of the peak intensity of B–N bonds (Fig. 2a), leading to the formation of $[LiNBH]_n$ chains *via* the intermolecular reaction between B–H bonds and N–H bonds as schematically illustrated in Fig. S4. These $[LiNBH]_n$ chains would be effectively crosslinked by the abundant strong Li–N ionic bonds between them, leading to the formation of a stable crosslinked and polymer-like structure [35,43]. The formation of the polymer-like $[LiNBH]_n$ chains could effectively enhance the structural integrity of the thus-built artificial SEI layers. It is worth noting that the characteristic XRD peaks related to LiZn alloy of LiNBH@Zn@Li electrode is obviously decreased compared with Zn@Li electrode, indicating the uniform coverage of polymer-like $[LiNBH]_n$ chains on the surface of Li metal anode (Fig. 2b). Top-view SEM images illustrate that the flat surface of Zn@Li electrode is well preserved after the formation of polymer-like $[LiNBH]_n$ chains (Fig. 1e and Fig. S5). Moreover, the energy-dispersive spectroscopy (EDS) elemental mapping results confirm that B, N, and Zn elements are uniformly dispersed inside of thus-built artificial layer (denoted as LiNBH@Zn layer), indicating the homogeneous distribution of LiZn alloy and polymer-like $[LiNBH]_n$ chains on the surface of LiNBH@Zn@Li anode (Fig. S5a). Accordingly,

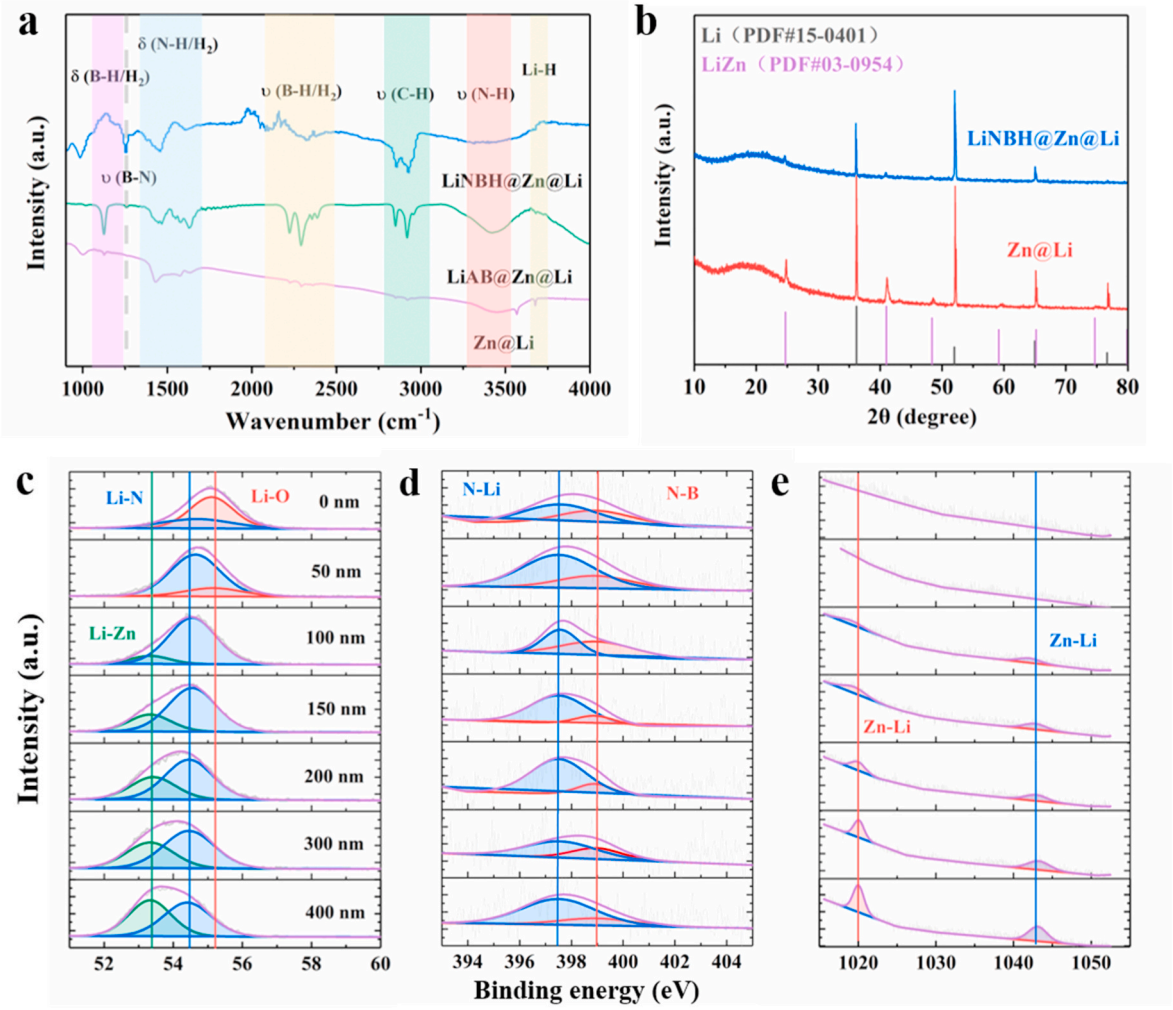

Fig. 2. (a) FTIR spectra of the top surface of the as-synthesized LiNBH@Zn@Li, LiAB@Zn@Li, and Zn@Li. (b) XRD patterns of the as-prepared LiNBH@Zn@Li and Zn@Li. In-depth XPS profile of Li 1s (c), N 1s (d), and Zn 1s (e) for the as-prepared LiNBH@Zn@Li.

cross-sectional SEM image and its line-scanning elemental analysis result illustrates the uniform distribution of B, N, and Zn elements of LiNBH@Zn@Li anode and the significant decrease of their signals upon the increase of depth, indicating a thickness of approximately 10 μm for the thus-built LiNBH@Zn layer (Fig. 1f and Fig. S5c), which is comparable to the thickness of LiZn alloys of Zn@Li anode.

The chemical environment of the surface of LiNBH@Zn@Li is investigated in detail by in-depth X-ray photo-electron spectroscopy (XPS) *via* continuous Ar ion etching (Fig. 2c–e). The characteristic peaks of 397.5 eV in the N 1s spectrum and 54.5 eV in the Li 1s spectrum could be assigned to N–Li bond of $[LiNBH]_n$ layer, and the characteristic peak of 399 eV in the N 1s spectrum could be attributed to N–B bonds of $[LiNBH]_n$ layer, which provides additional evidence to the formation of polymer-like $[LiNBH]_n$. The Li content of $[LiNBH]_n$ chains reaches 21.2 wt%, endowing it with a high Li ion conductivity of approximately 0.66 $\times 10^{-5}$ S cm^{-1} [35], which is several orders of magnitude of higher than that of the previously reported SEI layers. It could effectively promote uniform Li diffusion of the whole electrode. Upon the proceeding of etching down to 100 nm, the Zn–Li bonds could be detected in the high-resolution Zn 1s spectrum and Li 1s spectrum, indicating the formation of LiZn alloy beneath the polymer-like $[LiNBH]_n$ layer, which enables the protection of LiZn alloys from the corrosion of the electrolyte. More importantly, no obvious change of the relative signals of $[LiNBH]_n$ could be observed during the etching of thus-fabricated Li metal anodes, suggesting the uniform distribution of $[LiNBH]_n$ chains inside of LiNBH@Zn layer, which could not only facilitate the uniform Li diffusion due to the presence of massive Li–N bonds of $[LiNBH]_n$ but also restrain the volume change across the whole electrode due to the cross-linking of $[LiNBH]_n$ chains induced by the intramolecular reaction between B–H and N–H bonds [44–46]. As verified by atomic force microscopy (AFM) measurement, the average Young's modulus on the surface of LiNBH@Zn@Li is measured to be 2.5 GPa, much lower than that of Zn@Li (*i.e.*, ~5 GPa), which provides further evidence to the uniform coverage of polymer-like $[LiNBH]_n$ chains (Fig. S6).

The Li plating behavior of LiNBH@Zn@Li is first investigated using symmetric cells, with Zn@Li and bare Li metal anode included for comparison (Fig. S7). Based on the voltage-capacity profile, a large overpotential of ~320 mV could be observed for bare Li metal anode at 1 mA cm^{-2}, indicating the presence of a large nucleation barrier for pristine Li metal. As a result, induced by the lithiophilic nature of LiZn alloys [47–49], which could effectively reduce the nucleation barrier for Li plating, the nucleation overpotential is significantly decreased to 25 mV for Zn@Li anode. Interestingly, almost no nucleation overpotential could be detected for LiNBH@Zn@Li anode, validating the synergistic role of polymer-like $[LiNBH]_n$ chains and LiZn alloys in facilitating homogeneous Li deposition process. To unravel the synergistic effect of $[LiNBH]_n$ layer and LiZn alloys in stabilizing Li metal anodes, the electrochemical impedance spectra (EIS) of these symmetric cells is further conducted (Fig. 3a and b). Before cycling, the interfacial charge-transfer (R_{ct}) of bare Li metal anode reaches 177 Ω. Although this value could be

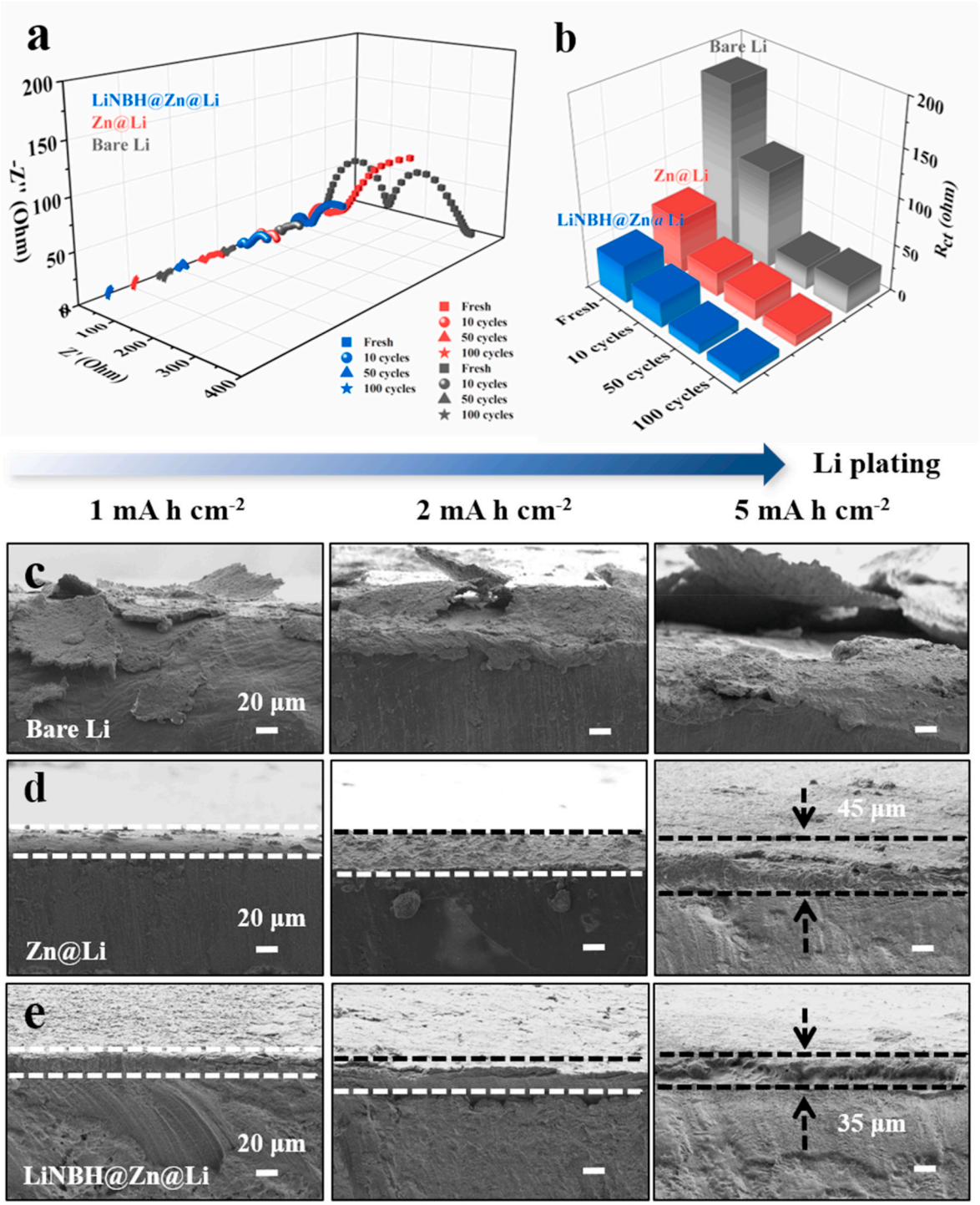

Fig. 3. (a) EIS results and (b) the corresponding value of R_{ct} for the as-fabricated LiNBH@Zn@Li and Zn@Li anode before and after cycling at 1 mA cm^{-2}. Side-view SEM images of bare Li (c), Zn@Li (d), and LiNBH@Zn@Li (e) after plating 1, 2, and 5 mA h cm^{-2} of Li at 1 mA cm^{-2}.

reduced to 60 Ω for Zn@Li owing to the uniform decoration of lithiophilic LiZn alloys, it is still much higher than that of LiNBH@Zn@Li (*i.e.*, ~41 Ω), indicative of improved interfacial conductivity and the suppressed corrosion by the electrolyte (Fig. S8). In addition, the exchange current density (I_0) for Li stripping and plating of LiNBH@Zn@Li is calculated to be 2.66 mA cm^{-2}, much higher than that of both bare Li (0.26 mA cm^{-2}) and Zn@Li (0.93 mA cm^{-2}), which directly demonstrates that the uniform introduction of polymer-like $[LiNBH]_n$ chains with high Li ion conductivity could effectively not only improve the structural integrity but also enhance the Li ion conductivity of the whole electrode (Fig. S10). To further prove the superior diffusion of Li^+ in the LiNBH@Zn@Li, the diffusion of Li^+ in the electrode is measured based on galvanostatic intermittent titration technique (GITT) (Fig. S11). The diffusion coefficient of Li^+ (D_{Li}) of LiNBH@Zn@Li is calculated to be approximately 9.44 × 10^{-8} cm^2 s^{-1}, much higher than that of Zn@Li anode (2.36 × 10^{-8} cm^2 s^{-1}), which confirms that the uniform introduction of polymer-like $[LiNBH]_n$ chains could enhance the diffusion of Li ions inside the LiNBH@Zn@Li anode. The improvement of both Li ion diffusion and electron conductivity due to the synergistic role of polymer-like $[LiNBH]_n$ chains with high Li ion conductivity and

lithiophilic LiZn alloys is capable of effectively promoting uniform Li stripping and plating process (Figs. S12 and S13). More importantly, after repeated Li stripping and plating process for 100 cycles, the R_{ct} value of LiNBH@Zn@Li anode is decreased to 9 Ω, much lower than that of Zn@Li, indicating the positive role of polymer-like $[LiNBH]_n$ chains in preserving structural integrity of Zn@Li, which leads to the formation of stable SEI layer with high charge-transfer kinetics. As a comparison, a clear increase of R_{ct} could observed for Li anode after only 100 cycles. Interestingly, similar phenomenon could be observed in symmetric cells when using carbonate-based electrolytes, indicating the structural stability of LiNBH@Zn@Li anode in various commercial electrolytes (Fig. S8d).

After the initial Li stripping process at 1 mA cm^{-2} with a fixed capacity of 1 mA h cm^{-2}, uneven Li stripping could be clearly observed for bare Li metal and, after the reverse Li plating process, the surface of bare Li metal is covered by dead Li with the observation of obvious cracks (Fig. 3c, Figs. S12 and S13). This phenomenon is significantly aggravated upon the increase of Li stripping and plating capacity to 5 mA h cm^{-2}, which directly demonstrates uneven Li stripping and plating process for bare Li metal. Interestingly, after the decoration of LiZn alloys with lithiophilic nature, the formation of dead Li is suppressed effectively due to the decrease of nucleation barrier for Li plating under

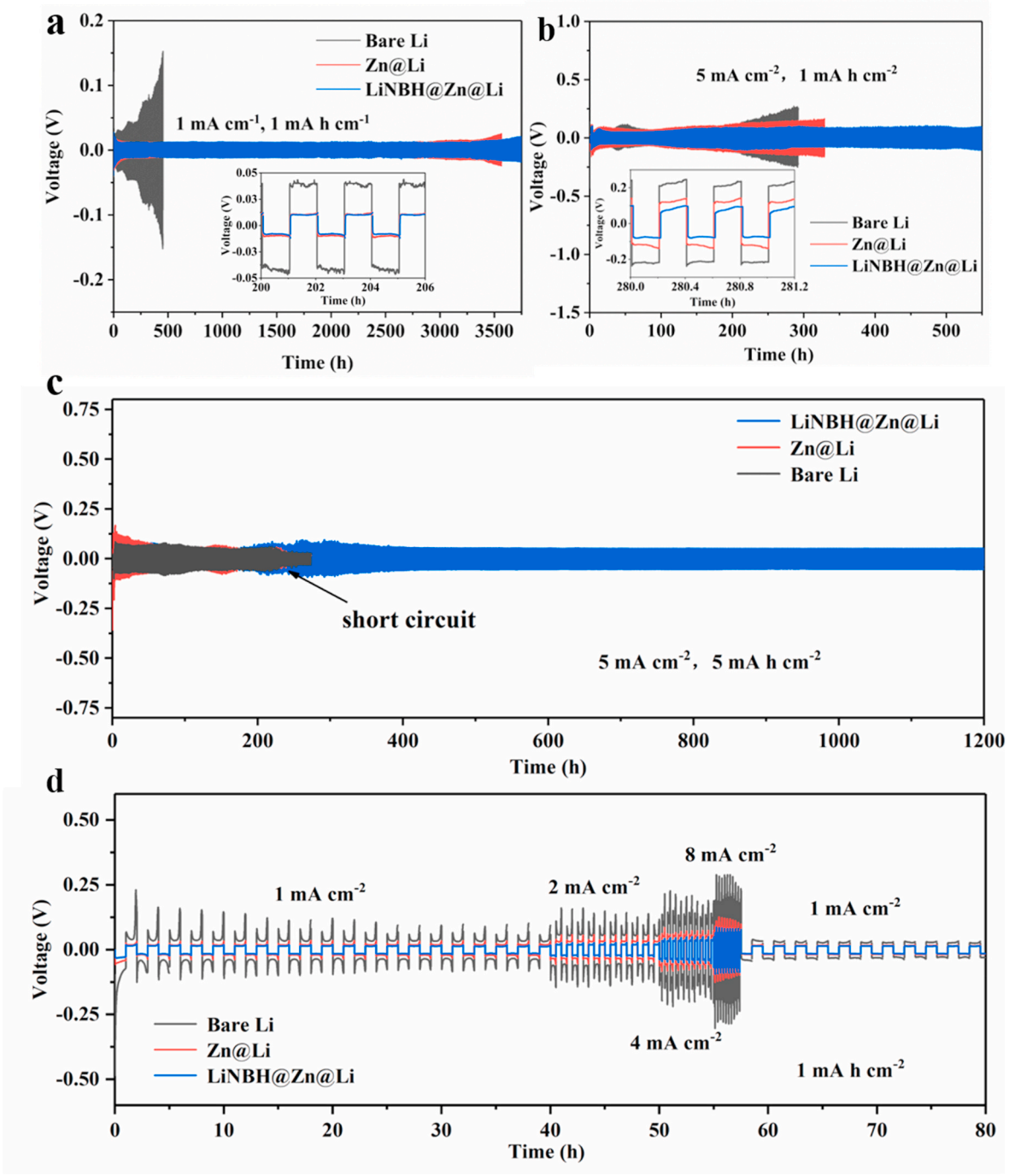

Fig. 4. Galvanostatic discharge and charge profiles of LiNBH@Zn@Li in symmetric cells at 1 mA cm^{-2} (a) and 5 mA cm^{-2} (b) with a fixed areal capacity at 1 mA h cm^{-2} and at 5 mA cm^{-2} with a fixed areal capacity at 5 mA h cm^{-2} (c), with Zn@Li and bare Li electrode included for comparison. (d) Rate performance of LiNBH@Zn@Li, Zn@Li, and bare Li in symmetric cells at various current densities.

identical condition. The thickness of LiZn alloys, however, is significantly increased to 45 μm after deposition of 5 mA h cm^{-2} of Li, corresponding to a volume change ratio of 350% (Fig. 3d). In strong contrast, under the protection and strengthening of polymer-like $[LiNBH]_n$ layer, the change of the thickness of artificial layers composed of LiZn alloys and polymer-like $[LiNBH]_n$ chains is limited to be 250%, which directly demonstrates that the homogeneous presence of polymer-like $[LiNBH]_n$ layer could facilitate the Li plating down to Li metal and hence alleviate the volume change of Li metal anodes (Fig. 3e). Moreover, induced by the synergistic role of lithiophilic LiZn alloys and polymer-like $[LiNBH]_n$ chains with high Li ion conductivity, a dendrite-free and smooth surface could still be observed for LiNBH@Zn@Li even upon increasing the applied capacity to 5 mA h cm^{-2}.

The cycling stability and reversibility of LiNBH@Zn@Li anode is subsequently evaluated by galvanostatic Li stripping and plating tests using symmetric cells with a fixed capacity of 1 mA h cm^{-2}. An obvious increase of overpotential could be observed for bare Li metal anode after cycling for only 200 h owing to the severe reaction between Li metal and electrolyte during repeated Li stripping and plating process (Fig. 4a). Owing to the uniform modification of LiZn alloys with lithiophilic nature, the cycling life of Zn@Li anode could be effectively prolonged to 3200 h. The continuous increase of overpotential, however, could still be detected for Zn@Li anode upon the proceeding of cycling, which could be attributed to the limited stability of LiZn alloys induced by its volume change upon long-term Li stripping and plating process

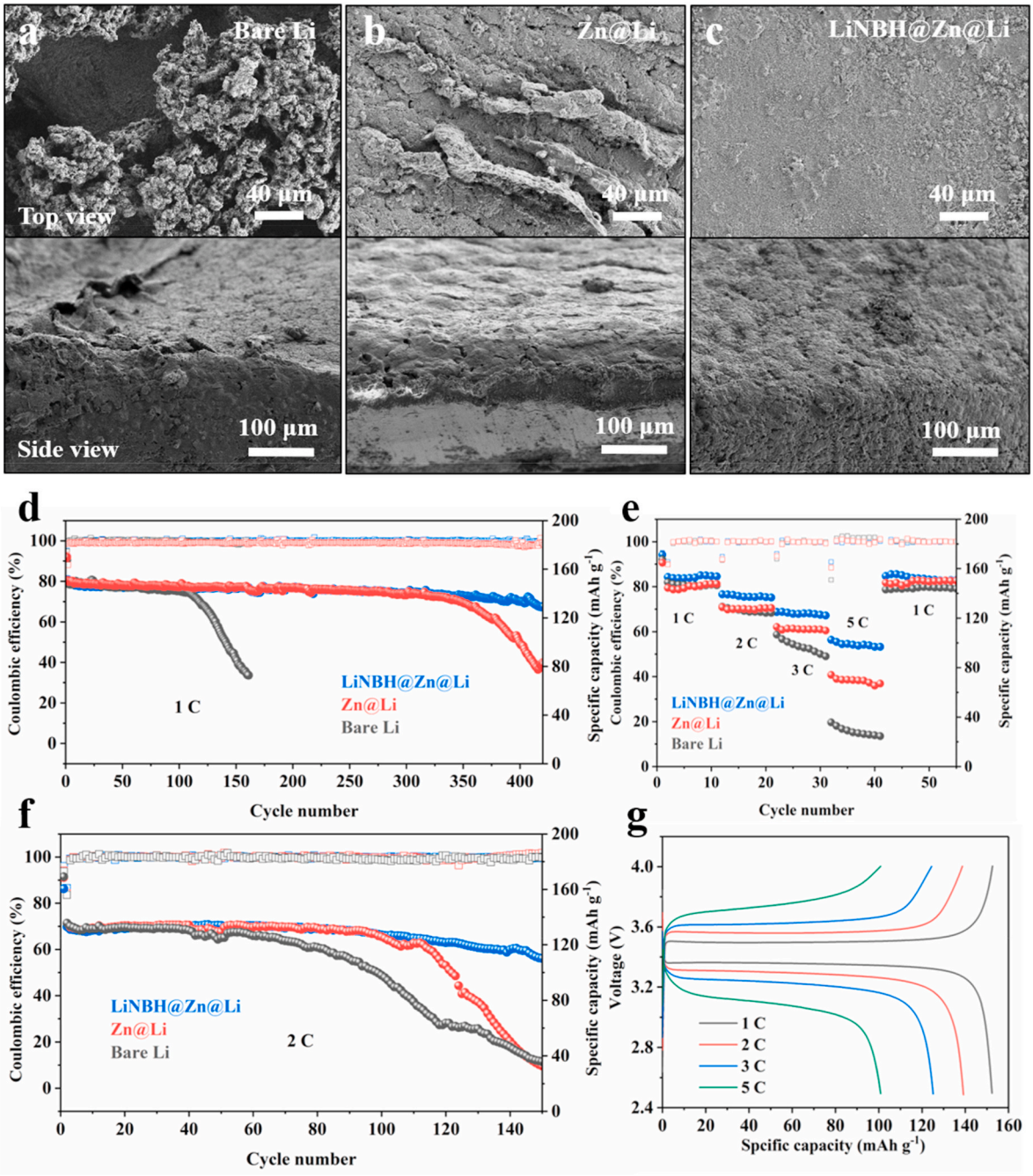

Fig. 5. SEM images of bare Li anode (a), Zn@Li (b), and LiNBH@Zn@Li (c) after 50 cycles at 2 mA cm^{-2} with a fixed areal capacity at 1 mA h cm^{-2}. (d and e) Cycling performance of LiNBH@Zn@Li||LFP, Zn@Li||LFP and bare Li||LFP full cells at 1 C and 2 C, respectively. (f) Rate capability of LiNBH@Zn@Li||LFP, Zn@Li||LFP, and bare Li||LFP full cells. (g) Charge/discharge profiles of LiNBH@Zn@Li||LFP full cells at various rates.

(Fig. 3d). In strong contrast, a stable voltage profile and ultralong lifespan for over 3500 h at a current density of 1 mA cm^{-2} could be obtained for LiNBH@Zn@Li anode (Fig. 4a). When the current density increases to 2 mA cm^{-2} and 5 mA cm^{-2}, LiNBH@Zn@Li anode still exhibits a stable cycling life of over 1000 h and 550 h, respectively, much superior than that of both bare Li metal anode and Zn@Li anode (Fig. 4b and Fig. S14). More impressively, upon increasing the current density to 5 mA cm^{-2} with an increasing capacity of 5 mA h cm^{-2}, a cycling lifespan of over 1200 h could still be achieved for the LiNBH@Zn@Li anode, which is among the best performance of Li metal anodes reported so far, while a sudden short circuit would be observed for bare Li after only 200 h of cycling (Fig. 4c). Interestingly, the overpotential of the LiNBH@Zn@Li anode slightly increases initially followed by the gradual decrease of the overpotential between 200 and 500 h, which could be widely observed during cycling process of various Li metal anodes reported previously [50–53]. It could be derived from the possible activation of Li metal anodes, which would lead to the gradual wetting of the electrolyte into the structure of LiNBH@Zn@Li anode, and the progressive structural modification of LiNBH@Zn@Li anode induced by its volume change towards stable cycling performance. Moreover, the LiNBH@Zn@Li anode displays a superior rate capability than both bare Li and Zn@Li anode under different current densities with a fixed capacity of 1 mA h cm^{-2}, indicating the enhanced kinetics for Li stripping and plating process (Fig. 4d). When the current density drops to 1 mA cm^{-2}, the overpotential of LiNBH@Zn@Li anode turns back to 12 mV immediately, demonstrating the excellent reversibility of Li stripping and plating process of LiNBH@Zn@Li anode. In addition, these symmetric cells are further measured in commercial carbonate electrolyte. LiNBH@Zn@Li anode exhibit a stable cycling performance for over 1700 h and 550 h at a current density of 1 mA cm^{-2} and 2 mA cm^{-2}, respectively, with a fixed capacity of 1 mA h cm^{-2} (Figs. S15 and S16a). Even at a high current density of 3 mA cm^{-2} with a large areal capacity of 3 mA h cm^{-2}, LiNBH@Zn@Li anode maintains a stable discharging and charging process for over 300 h in carbonate-based electrolyte, while the voltage profile of bare Li||bare Li cells exhibit huge fluctuation after cycling for only 100 h (Fig. S16b).

The morphology change is further investigated to directly illustrate the effect of LiNBH@Zn@Li in suppressing the growth of Li dendrites. As shown in Fig. 5a, owing to the inhomogeneous Li plating, obvious formation of Li dendrites and cracks could be observed after 50 cycles of Li stripping and plating process. After the modification with lithiophilic LiZn alloys, the growth of Li dendrites could be effectively suppressed upon the proceeding of Li stripping and plating process. The formation of cracks, however, is still verified for Zn@Li anode owing to the thus-induced stress by repeated volume change of LiZn alloys during cycling (Fig. 5b). By comparison, LiNBH@Zn@Li anode displays a relatively smooth and dense surface without the observation of any Li dendrites (Fig. 5c), which is comparable to the morphology of the freshly fabricated electrode. As schematically illustrated in Fig. S17, this sharp contrast directly validates the long-term stability of the as-prepared LiNBH@Zn@Li anode towards dendrite-free cycling performance, which could be attributed to the synergistic role of lithiophilic LiZn alloys in lowering the nucleation barrier of Li plating and polymer-like $[LiNBH]_n$ chains with high Li ion conductivity in regulating Li ion diffusion towards Li plating down into lithiophilic LiZn allys and alleviating the volume change of LiZn alloys.

The specific capacity of LiNBH@Zn@Li with a thickness of 200 μm was first evaluated by galvanostatic charging method to confirm the ratio of Zn and $[LiNBH]_n$ polymers in the electrode. The voltage profile shows that a high specific capacity of 3582 mA h g^{-1} could be obtained, equaling to a weight ratio of 92.8 wt% for activated Li in the as-prepared LiNBH@Zn@Li electrode, which is close to the theoretical specific capacity of Li metal (Fig. S18). In order to verify the feasibility of LiNBH@Zn@Li anode for practical application, full cells coupled with commercial $LiFePO_4$ (LFP; ~10.5 mg cm^{-2}) cathode (denoted as LiNBH@Zn@Li||LFP) are assembled for investigating electrochemical performance. Long-term cycling performance validates that bare Li||LFP full cells exhibit a sharp capacity degradation after only 110 cycles (Fig. 5d and Fig. S19) owing to the tremendous growth of Li dendrites and dead Li (Fig. S20a). Although the cycling life of Zn@Li||LFP full cells could be extended to 330 cycles, a sharp decrease of specific capacity could be subsequently observed for Zn@Li||LFP full cells owing to the limited role of lithiophilic LiZn alloys in suppressing the growth of dead Li (Fig. S20b), delivering a capacity retention of 66% after 400 cycles. By comparison, a specific capacity of 133 mA h g^{-1}, corresponding to a capacity retention of 88%, could still be achieved for LiNBH@Zn@Li|| LFP full cell after 400 cycles, which could be attributed to the uniform Li plating and stripping process of LiNBH@Zn@Li anode (Figs. S20c and f). Upon cycling at a high rate of 2 C, bare Li||LFP full cells exhibit a sharply decreased capacity of 80 mA h g^{-1} after only 110 cycles. On the contrary, LiNBH@Zn@Li||LFP full cells maintain a high capacity retention of 82.8% even after 150 cycles (Fig. 5e and Fig. S19b). In addition, rate capability verifies that LiNBH@Zn@Li||LFP full cells present higher reversible specific capacity of 149, 138, 121, and 101 mA h g^{-1} at 1 C, 2 C, 3 C, and 5 C, respectively, than that of both Zn@Li||LFP full cells and Li||LFP full cells (Fig. 5f). Moreover, when the current density is returned back to 1 C, the reversible capacity of LiNBH@Zn@Li anode could be completely recovered, indicating stable reversibility of the thus-assembled full cells. The enhancement of reversible capacity of LiNBH@Zn@Li||LFP full cells could be attributed to the superior kinetics of LiNBH@Zn@Li anode as validated by the lower overpotential in the discharge and charge profiles at various current densities (Fig. 5g). The advantage of LiNBH@Zn@Li anode for practical application is further investigated in Li–S cells, which have been regarded as one of the most promising next-generation rechargeable batteries [54–57]. The specific capacity of Li||S full cells dramatically drop to 586 mA h g^{-1} after only 100 cycles at the rate of 1 C (Fig. S21). In strong contrast, LiNBH@Zn@Li||S full cells deliver a high specific capacity of 799 mA h g^{-1} under the identical conditions and a reversible capacity of 607 mA h g^{-1} could still be obtained after over 400 cycles.

4. Conclusion

In conclusion, we develop a facile strategy to fabricate a stable artificial SEI layer composed of lithiophlic LiZn alloy under the protection and strengthening of polymer-like $[LiNBH]_n$ chains with high Li ion conductivity to realize long-term dendrite-free Li meal anode. The lithiophilic LiZn alloys, serving as homogeneous nucleation sites, effectively reduce the nucleation barrier for Li plating and hence promote uniform Li plating and stripping process based on the reversible solid solution-based alloying reaction. More importantly, the homogeneous layer of polymer-like $[LiNBH]_n$ chains with high Li ion conductivity that are uniformly built inside of LiZn alloys and on the surface of LiZn alloys is able to promote Li diffusion down into LiZn alloys towards dendrite-free Li plating and simultaneously alleviate the volume change of LiZn alloys towards long-term structural integrity during repeated Li stripping and plating process. As a result, the as-fabricated LiNBH@Zn@Li anode exhibits a very stable voltage profile and ultralong lifespan for over 3500 h at a current density of 1 mA cm^{-2} with a fixed capacity of 1 mA h cm^{-2}. More impressively, when the current density is increased to 5 mA cm^{-2} with a deep Li plating and stripping capacity of 5 mA h cm^{-2}, the LiNBH@Zn@Li anode is still capable of delivering stable cycling performance for 1200 h. Moreover, when coupling LiNBH@Zn@Li anode with commercial LFP cathode, the thus-assembled full cells could stably operate for over 679 h with a capacity retention of 88% at 1 C after 400 cycles. This work provides a feasible method to realize Li metal anodes with long-term cycling stability, which could be further extended to the protection of Na or K metal anodes.

CRediT authorship contribution statement

Yongfang Lai: Investigation, Formal analysis, Writing – original draft. **Hongyu Zhang:** Investigation, Methodology. **Guanglin Xia:** Supervision, Conceptualization, Methodology, Writing – review & editing. **Xuebin Yu:** Supervision, Conceptualization, Methodology, Writing – review & editing.

Declaration of competing interest

The authors declare that they have no known competing financial interests or personal relationships that could have appeared to influence the work reported in this paper.

Data availability

Data will be made available on request.

Acknowledgements

This work was partially supported by the National Key R&D Program of China (No. 2020YFA0406204), National Science Fund for Distinguished Young Scholars (51625102), the National Natural Science Foundation of China (51971065, 51901045, U2130208), the Science and Technology Commission of Shanghai Municipality (No. 21ZR1407500), and the Innovation Program of Shanghai Municipal Education Commission (2019-01-07-00-07-E00028), and the Programs for Professor of Special Appointment (Eastern Scholar) at Shanghai Institutions of Higher Learning.

Appendix A. Supplementary data

Supplementary data to this article can be found online at https://doi.org/10.1016/j.jpowsour.2022.231839.

References

[1] Z.A. Ghazi, Z. Sun, C. Sun, F. Qi, B. An, F. Li, H.-M. Cheng, Key aspects of lithium metal anodes for lithium metal batteries, Small 15 (2019), 1900687.
[2] J.M. Tarascon, M. Armand, Issues and challenges facing rechargeable lithium batteries, Nature 414 (2001) 359–367.
[3] V. Etacheri, R. Marom, R. Elazari, G. Salitra, D. Aurbach, Challenges in the development of advanced Li-ion batteries: a review, Energy Environ. Sci. 4 (2011) 3243–3263.
[4] P. Albertus, S. Babinec, S. Litzelman, A. Newman, Status and challenges in enabling the lithium metal electrode for high-energy and low-cost rechargeable batteries, Nat. Energy 3 (2018) 16–21.
[5] D.R. Ely, R.E. Garcia, Heterogeneous nucleation and growth of lithium electrodeposits on negative electrodes, J. Electrochem. Soc. 160 (2013) A662–A668.
[6] K. Yan, Z. Lu, H.-W. Lee, F. Xiong, P.-C. Hsu, Y. Li, J. Zhao, S. Chu, Y. Cui, Selective deposition and stable encapsulation of lithium through heterogeneous seeded growth, Nat. Energy 1 (2016), 16010.
[7] A. Pei, G. Zheng, F. Shi, Y. Li, Y. Cui, Nanoscale nucleation and growth of electrodeposited lithium metal, Nano Letters, Nano Lett. 17 (2017) 1132–1139.
[8] Y. Liu, Y. Zhu, Y. Cui, Challenges and opportunities towards fast-charging battery materials, Nat. Energy 4 (2019) 540–550.
[9] D. Aurbach, E. Zinigrad, H. Teller, P. Dan, Factors which limit the cycle life of rechargeable lithium (metal) batteries, J. Electrochem. Soc. 147 (2000) 1274–1279.
[10] X.-B. Cheng, R. Zhang, C.-Z. Zhao, Q. Zhang, Toward safe lithium metal anode in rechargeable batteries: a review, Chem. Rev. 117 (2017) 10403–10473.
[11] M.M. Thackeray, C. Wolverton, E.D. Isaacs, Electrical energy storage for transportation-approaching the limits of, and going beyond, lithium-ion batteries, Energy Environ. Sci. 5 (2012) 7854–7863.
[12] E. Peled, D. Golodnitsky, G. Ardel, Advanced model for solid electrolyte interphase electrodes in liquid and polymer electrolytes, J. Electrochem. Soc. 144 (1997) L208–L210.
[13] K. Ushirogata, K. Sodeyama, Z. Futera, Y. Tateyama, Y. Okunoa, Near-shore aggregation mechanism of electrolyte decomposition products to explain solid electrolyte interphase formation, J. Electrochem. Soc. 162 (2015) A2670–A2678.
[14] Y.S. Cohen, Y. Cohen, D. Aurbach, Micromorphological studies of lithium electrodes in alkyl carbonate solutions using in situ atomic force microscopy, J. Phys. Chem. B 104 (2000) 12282–12291.
[15] Z. Liang, G. Zheng, C. Liu, N. Liu, W. Li, K. Yan, H. Yao, P.-C. Hsu, S. Chu, Y. Cui, Polymer nanofiber-Guided uniform lithium deposition for battery electrodes, Nano Lett. 15 (2015) 2910–2916.
[16] S. Matsuda, Y. Kubo, K. Uosaki, S. Nakanishi, Insulative microfiber 3D matrix as a host material minimizing volume change of the anode of Li metal batteries, ACS Energy Lett. 2 (2017) 924–929.
[17] X.-B. Cheng, T.-Z. Hou, R. Zhang, H.-J. Peng, C.-Z. Zhao, J.-Q. Huang, Q. Zhang, Dendrite-free lithium deposition induced by uniformly distributed lithium ions for efficient lithium metal batteries, Adv. Mater. 28 (2016) 2888–2895.
[18] N.-W. Li, Y.-X. Yin, C.-P. Yang, Y.-G. Guo, An artificial solid electrolyte interphase layer for stable lithium metal anodes, Adv. Mater. 28 (2016) 1853–1858.
[19] Y. Liu, D. Lin, P.Y. Yuen, K. Liu, J. Xie, R.H. Dauskardt, Y. Cui, An artificial solid electrolyte interphase with high Li-Ion conductivity, mechanical strength, and flexibility for stable lithium metal anodes, Adv. Mater. 29 (2017), 1605531.
[20] H.-K. Jing, L.-L. Kong, S. Liu, G.-R. Li, X.-P. Gao, Protected lithium anode with porous Al_2O_3 layer for lithium-sulfur battery, J. Mater. Chem. 3 (2015) 12213–12219.
[21] H.Y. Zhang, S. Ju, G.L. Xia, X.B. Yu, Identifying the positive role of lithium hydride in stabilizing Li metal anodes, Sci. Adv. 8 (2022), eabl8245.
[22] Y. Lei, S. Ju, J. Liu, G.L. Xia, Z.P. Guo, X.B. Yu, Synergistic effect of lithiophilic Zn nanoparticles and N-doping for stable Li metal anodes, J. Energy Chem. 65 (2022) 439–447.
[23] S. Ye, L. Wang, F. Liu, P. Shi, H. Wang, X. Wu, Y. Yu, g-C_3N_4 derivative artificial organic/inorganic composite solid electrolyte interphase layer for stable lithium metal anode, Adv. Energy Mater. 10 (2020), 2002647.
[24] R. Tao, X. Bi, S. Li, Y. Yao, F. Wu, Q. Wang, C. Zhang, J. Lu, Kinetics tuning the electrochemistry of lithium dendrites formation in lithium batteries through electrolytes, ACS Appl. Mater. Interfaces 9 (2017) 7003–7008.
[25] J. Wang, F. Lin, H. Jia, J. Yang, C.W. Monroe, Y. NuLi, Towards a safe lithium-sulfur battery with a flame-inhibiting electrolyte and a sulfur-based composite cathode, Angew. Chem. Int. Ed. 53 (2014) 10099–10104.
[26] F. Ding, W. Xu, G.L. Graff, J. Zhang, M.L. Sushko, X. Chen, Y. Shao, M. H. Engelhard, Z. Nie, J. Xiao, X. Liu, P.V. Sushko, J. Liu, J.-G. Zhang, Dendrite-free lithium deposition via self-healing electrostatic shield mechanism, J. Am. Chem. Soc. 135 (2013) 4450–4456.
[27] H. Dai, X. Gu, J. Dong, C. Wang, C. Lai, S. Sun, Stabilizing lithium metal anode by octaphenyl polyoxyethylene-lithium complexation, Nat. Commun. 11 (2020) 643.
[28] L.-P. Hou, N. Yao, J. Xie, P. Shi, S.-Y. Sun, C.-B. Jin, C.-M. Chen, Q.-B. Liu, B.-Q. Li, X.-Q. Zhang, Q. Zhang, Modification of nitrate ion enables stable solid electrolyte interphase in lithium metal batteries, Angew. Chem. Int. Ed. 61 (2022), e202201406.
[29] M.S. Kim, J.-H. Ryu, Deepika, Y.R. Lim, I.W. Nah, K.-R. Lee, L.A. Archer, W. Il Cho, Langmuir–blodgett artificial solid-electrolyte interphases for practical lithium metal batteries, Nat. Energy 3 (2018) 889–898.
[30] J.W. Choi, D. Aurbach, Promise and reality of post-lithium-ion batteries with high energy densities, Nat. Rev. Mater. 1 (2016), 16013.
[31] L. Wang, S. Fu, T. Zhao, J. Qian, N. Chen, L. Li, F. Wu, R. Chen, *In situ* formation of a LiF and Li-Al alloy anode protected layer on a Li metal anode with enhanced cycle life, J. Mater. Chem. 8 (2020) 1247–1253.
[32] S. Xia, X. Zhang, C. Liang, Y. Yu, W. Liu, Stabilized lithium metal anode by an efficient coating for high-performance Li-S batteries, Energy Storage Mater. 24 (2020) 329–335.
[33] S. Li, J. Huang, Y. Cui, S. Liu, Z. Chen, W. Huang, C. Li, R. Liu, R. Fu, D. Wu, A robust all-organic protective layer towards ultrahigh-rate and large-capacity Li metal anodes, Nat. Nanotechnol. 17 (2022) 613–621.
[34] J. Zeng, Q. Liu, D. Jia, R. Liu, S. Liu, B. Zheng, Y. Zhu, R. Fu, D. Wu, A polymer brush-based robust and flexible single-ion conducting artificial SEI film for fast charging lithium metal batteries, Energy Storage Mater. 41 (2021) 697–702.
[35] Z. Wang, Y. Wang, Z. Zhang, X. Chen, W. Lie, Y.-B. He, Z. Zhou, G.L. Xia, Z.P. Guo, Building artificial solid-electrolyte interphase with uniform intermolecular ionic bonds toward dendrite-free lithium metal anodes, Adv. Funct. Mater. 30 (2020), 2002414.
[36] D. Bresser, F. Mueller, M. Fiedler, S. Krueger, R. Kloepsch, D. Baither, M. Winter, E. Paillard, S. Passerini, Transition-metal-doped zinc oxide nanoparticles as a new lithium-ion anode material, Chem. Mater. 25 (2013) 4977–4985.
[37] Y. An, Y. Tian, Y. Li, C. Wei, Y. Tao, Y. Liu, B. Xi, S. Xiong, J. Feng, Y. Qian, Heteroatom-doped 3D porous carbon architectures for highly stable aqueous zinc metal batteries and non-aqueous lithium metal batteries, Chem. Eng. J. 400 (2020), 125843.
[38] C. Sun, Y. Li, J. Jin, J. Yang, Z. Wen, ZnO nanoarrays modified nickel foam as a lithiophilic skeleton to regulate lithium deposition for lithium-metal batteries, J. Mater. Chem. 7 (2019) 7752–7759.
[39] H.Y. Zhang, S. Ju, G.L. Xia, D.L. Sun, X.B. Yu, Dendrite-free Li-metal anode enabled by dendritic structure, Adv. Funct. Mater. 31 (2021), 2009712.
[40] W. Li, R.H. Scheicher, C.M. Araujo, G. Wu, A. Blomqvist, C. Wu, R. Ahuja, Y. P. Feng, P. Chen, Understanding from first-principles why $LiNH_2BH_3{\cdot}NH_3BH_3$ shows improved dehydrogenation over $LiNH_2BH_3$ and NH_3BH_3, J. Phys. Chem. C 114 (2010) 19089–19095.
[41] C.Z. Wu, G.T. Wu, Z.T. Xiong, W.I.F. David, K.R. Ryan, M.O. Jones, P.P. Edwards, H.L. Chu, P. Chen, Stepwise phase transition in the formation of lithium amidoborane, Inorg. Chem. 49 (2010) 4319–4323.
[42] T.B. Lee, M.L. McKee, Mechanistic study of $LiNH_2BH_3$ formation from $(LiH)_4$ + NH_3BH_3 and subsequent dehydrogenation, Inorg. Chem. 48 (2009) 7564–7575.
[43] D.Y. Kim, N.J. Singh, H.M. Lee, K.S. Kim, Hydrogen-release mechanisms in lithium amidoboranes, Chem. Eur J. 15 (2009) 5598–5604.

[44] T. He, H. Wu, G. Wu, Z. Li, W. Zhou, X. Ju, D. Xie, P. Chen, Lithium amidoborane hydrazinates: synthesis, structure and hydrogen storage properties, J. Mater. Chem. 3 (2015) 10100–10106.
[45] Z. Xiong, C.K. Yong, G. Wu, P. Chen, W. Shaw, A. Karkamkar, T. Autrey, M. O. Jones, S.R. Johnson, P.P. Edwards, W.I.F. David, High-capacity hydrogen storage in lithium and sodium amidoboranes, Nat. Mater. 7 (2008) 138–141.
[46] X. Kang, Z. Fang, L. Kong, H. Cheng, X. Yao, G. Lu, P. Wang, Ammonia borane destabilized by lithium hydride: an advanced on-board hydrogen storage material, Adv. Mater. 20 (2008) 2756.
[47] H. Shi, X. Ren, J. Lu, C. Dong, J. Liu, Q. Yang, J. Chen, Z.-S. Wu, Dual-functional atomic zinc decorated hollow carbon nanoreactors for kinetically accelerated polysulfides conversion and dendrite free lithium sulfur batteries, Adv. Energy Mater. 10 (2020), 2002271.
[48] S.-S. Chi, Q. Wang, B. Han, C. Luo, Y. Jiang, J. Wang, C. Wang, Y. Yu, Y. Deng, Lithiophilic Zn sites in porous CuZn alloy induced uniform Li nucleation and dendrite-free Li metal deposition, Nano Lett. 20 (2020) 2724–2732.
[49] Y. Ouyang, C. Cui, Y. Guo, Y. Wei, T. Zhai, H. Li, In situ formed LiZn alloy skeleton for stable lithium anodes, ACS Appl. Mater. Interfaces 12 (2020) 25818–25825.
[50] M.S. Kim, Deepika, S.H. Lee, M.-S. Kim, J.-H. Ryu, K.-R. Lee, L.A. Archer, W.I. Cho, Enabling reversible redox reactions in electrochemical cells using protected LiAl intermetallics as lithium metal anodes, Sci. Adv. 5 (2019), eaax5587.
[51] Y. Zhong, F. Lin, M. Wang, Y. Zhang, Q. Ma, J. Lin, Z. Feng, H. Wang, Metal organic framework derivative improving lithium metal anode cycling, Adv. Funct. Mater. 30 (2020), 1907579.
[52] J. Xiao, P. Zhai, Y. Wei, X. Zhang, W. Yang, S. Cui, C. Jin, W. Liu, X. Wang, H. Jiang, Z. Luo, X. Zhang, Y. Gong, In-situ formed protecting layer from organic/inorganic concrete for dendrite-free lithium metal anodes, Nano Lett. 20 (2020) 3911–3917.
[53] G. Wang, C. Chen, Y. Chen, X. Kang, C. Yang, F. Wang, Y. Liu, X. Xiong, Self-stabilized and strongly adhesive supramolecular polymer protective layer enables ultrahigh-rate and large-capacity lithium-metal anode, Angew. Chem. Int. Ed. 59 (2020) 2055–2060.
[54] Y.-X. Yin, S. Xin, Y.-G. Guo, L.-J. Wan, Lithium-sulfur batteries: electrochemistry, materials, and prospects, Angew. Chem., Int. Ed. 52 (2013) 13186–13200.
[55] R. Fang, S. Zhao, Z. Sun, W. Wang, H.-M. Cheng, F. Li, More reliable lithium-sulfur batteries: status, solutions and prospects, Adv. Mater. 29 (2017), 1606823.
[56] A. Fu, C. Wang, F. Pei, J. Cui, X. Fang, N. Zheng, Recent advances in hollow porous carbon materials for lithium-sulfur batteries, Small 15 (2019), 1804786.
[57] X. Li, X. Sun, Interface design and development of coating materials in lithium-sulfur batteries, Adv. Funct. Mater. 28 (2018), 1801323.